Physics-Based Earthquake Simulations of the Anninghe-Zemuhe-Daliangshan-Xiaojiang Fault system in the Southwestern China

Shangwu Song[1], Ke Jia[2*], Yu Hou[3], Ming Hao[1], Qingliang Wang[1], Jianping Wu[4], Shiyong Zhou[3]

1 The Second Monitoring Center, China Earthquake Administration, Xi'an 710043, China.

2 The School of Automation, Northwestern Polytechnical University, Xi'an 710129, China

3 The School of Earth and Space Sciences, Peking University, Beijing 100871, China

4 Institute of Geophysics, China Earthquake Administration, No.5 Minzu Daxue Nan Road, Haidian District, Beijing 100086, China

*Corresponding authors: jk@nwpu.edu.cn

Key points:

1. We propose a fault model for the Anninghe-Zemuhe-Daliangshan-Xiaojiang faults constrained by GPS data.
2. We Simulate a 20ka years of synthetic seismic catalog based on present fault behavior by applying a physics-based earthquake simulator.
3. We obtain the occurrence rate and mean recurrence interval of strong earthquakes (M7) on the AZDX faults

Abstract

Seismic hazard evaluation is important for urban construction, earthquake disaster prevention and mitigation. However, because of the long recurrence times of large earthquakes (hundreds to thousands of years), seismic hazard assessment based on relatively short-term (tens of years) observational seismic catalog is difficult. Synthetic seismic catalogs provide a useful way to obtain long-term seismic hazard. Based on Coulomb failure criterion, we apply a quasi-static physics-based earthquake simulator (Virtual Quake) in a tectonically complicated region with several major faults, namely the Anninghe, Zemuhe, Daliangshan and Xiaojiang faults, in the Southwestern China. Slip rates of those major faults are constrained by the GPS data, and frictions are constrained by the laboratory experiments. Considering the stress interactions among the fault system, a synthetic catalog over 20, 000 years is simulated. The simulated catalog shows consistence with the observed seismicity in spatial distribution of large earthquakes, b value and mean seismic rate. The synthetic catalog also shows that the mean intervals of M 7.0 earthquakes for the Anninghe, Zemuhe, Daliangshan and Xiaojiang faults are 299a, 867a, 361a and 90a, respectively. Our results provide a helpful index to evaluate seismic hazard in such a complicated region.

Plain Language Summary

Evaluating Seismic hazard is important for building code, risk prevention and mitigation. Because the large earthquakes are rare, the modern observed earthquake catalogs are too short for seismic hazard evaluation. Thus, numerical simulations are used to obtain synthetic earthquake catalog and evaluate seismic hazard. Here, we simulate earthquake sequence in the Anninghe-Zemuhe-Daliangshan-Xiaojiang fault system, southwestern China, under a physics-based framework, which considers stress transfer among major faults. Thus, we obtain a long-term synthetic catalog over 20,000 years. By comparing spatial distributions of large earthquakes, b values and mean seismic rates of the synthetic catalog and observed catalog, we find that the synthetic catalog is consistence with the observed catalog, and the mean occurrence times of M 7.0 earthquakes for the Anninghe, Zemuhe, Daliangshan and Xiaojiang faults are 299, 867, 361 and 90 years, respectively. Our results can help to evaluate long-term seismic hazard in a multiple-fault system.

1. Introduction

Seismic hazard assessment is a crucial issue for science community and public interest. Although rapid development of modern earthquake observations is improved, the observed seismic catalog (normally tens of years) is too short to accurately evaluate earthquake hazards (Field, 2019), especially for strong earthquakes whose recurrences are typically hundreds or even thousands of years for continental earthquakes (Liu and Stein, 2011). Recently, synthetic seismic catalogs, as long as tens of thousands years, provide an alternative way to estimate long term seismic hazard (Robinson and Benites, 1996; Shaw *et al.*, 2018; Zhou, 2008; Zöller and Ben-Zion, 2014). It is also nature that synthetic seismic catalogs can be applied to extract spatiotemporal features of strong earthquakes, magnitude frequency distributions (b value) of earthquakes, large earthquakes' recurrence and earthquake probabilities. Meanwhile, multiple faults interactions in a long period play an important role in seismic hazard assessment, especially for regions with many active faults (e.g., California, southwestern China) (Shaw *et al.*, 2018; Sun *et al.*, 2020). However, such interactions, especially for strong earthquakes, are also rare in modern seismic catalogs. Thus, considering multiple fault interactions, a reliable synthetic seismic catalog in a fault system can be simulated to assess long-term seismic hazard.

Typically, physics-based and statistic-based methods are two ways to generate synthetic seismic catalogs. Physics-based methods usually construct a fault system which obeys frictional laws under tectonic loading determined by observations. Then, the timing and locations of rupture failures are determined by Coulomb stress failure law and stress transfers among earthquakes are also considered to simulate real earthquake interactions. With the time increases, multiple cycles of earthquakes can be generated. Statistic-based methods apply mathematic principles (e.g., point process) to characteristic earthquakes based on several statistical laws which earthquakes obey (e.g., Gutenberg-Richter law, Omori-Utsu law). Once the parameters of mathematic models are estimated

using observed catalog, synthetic catalogs can be generated by simulating the seismicity in a certain period. While the statistic-based simulations hardly capture the mechanisms of earthquake rupture and interaction, the synthetic catalogs using physics-based methods are more preferred in evaluating seismic hazards.

Synthetic catalogs using physics-based simulation has been rapidly developed in the past years (Ben-Zion, 1996; Console *et al.*, 2021; Hou *et al.*, 2020; Sun *et al.*, 2020; Zhou *et al.*, 2006). Tullis (2012) introduced four physics-based methods to generate synthetic catalogs, namely ALLCAL (Ward, 2012), Vitrual California earthquake simulator (Sachs *et al.*, 2012), RSQsim (Richards-Dinger and Dieterich, 2012) and ViscoSim (Pollitz, 2012). Although constitutive descriptions of fault friction vary among those four models, their simulated catalogs for the allcal2 California fault model show agreement with each other in general (e.g., frequency-magnitude distribution, moment and events rate), and also match the observed catalog (Tullis *et al.*, 2012). Virtual Quake (Yoder *et al.*, 2015) is proposed as a generalization of the Virtual California earthquake simulator, and can model any arbitrary fault system. Thus, the primary advantages of using VQ are conveniences in fault model setup, easily calculations of earthquake probabilities and partition of the simulated catalog. VQ has been successfully applied in several tectonic regions to investigate statistic characteristics of synthetic catalogs (Yoder *et al.*, 2015), seismic hazard forecast (Console *et al.*, 2018; Khodaverdian *et al.*, 2016b), precursory seismicity (Christophersen *et al.*, 2017) and friction law (Schultz *et al.*, 2018).

The Anninghe-Zemuhe-Daliangshan-Xiaojiang (AZDX) fault system, consisting of Anninghe, Zemuhe, Daliangshan and Xiaojiang faults, locates at the eastern boundary of the Tibetan Plateau (Figure 1). Resulting from the collision between the India and Eurasia plate, the AZDX faults are sinistral strike-slip faults, with slip rates of 4.0mm/a to 13.8mm/a from the northern part to southern part. A lot of major historical earthquakes have been occurred along the AZDX fault system, and the largest one was the 1833 September 6^{th} M8.0 event at the Xiaojiang fault (Wen *et al.*, 2008a). Wen *et al.* (2008a) has documented rupture pattern of tens of historical earthquakes along the AZDX fault system in details, providing a reliable catalog to assess seismic hazard in this region. However, such historical catalog (~600 years) is still too short for long-term seismic hazard evaluation due to the long recurrence intervals (250-600 years) of M7.0 earthquakes in the AZDX fault system (Wen *et al.*, 2008a). According to GPS, InSAR, seismic observations and simulation results, recent studies have shown that the seismic hazard of the AZDX fault system may be high (Jiang *et al.*, 2015b; Yao and Yang, 2021).

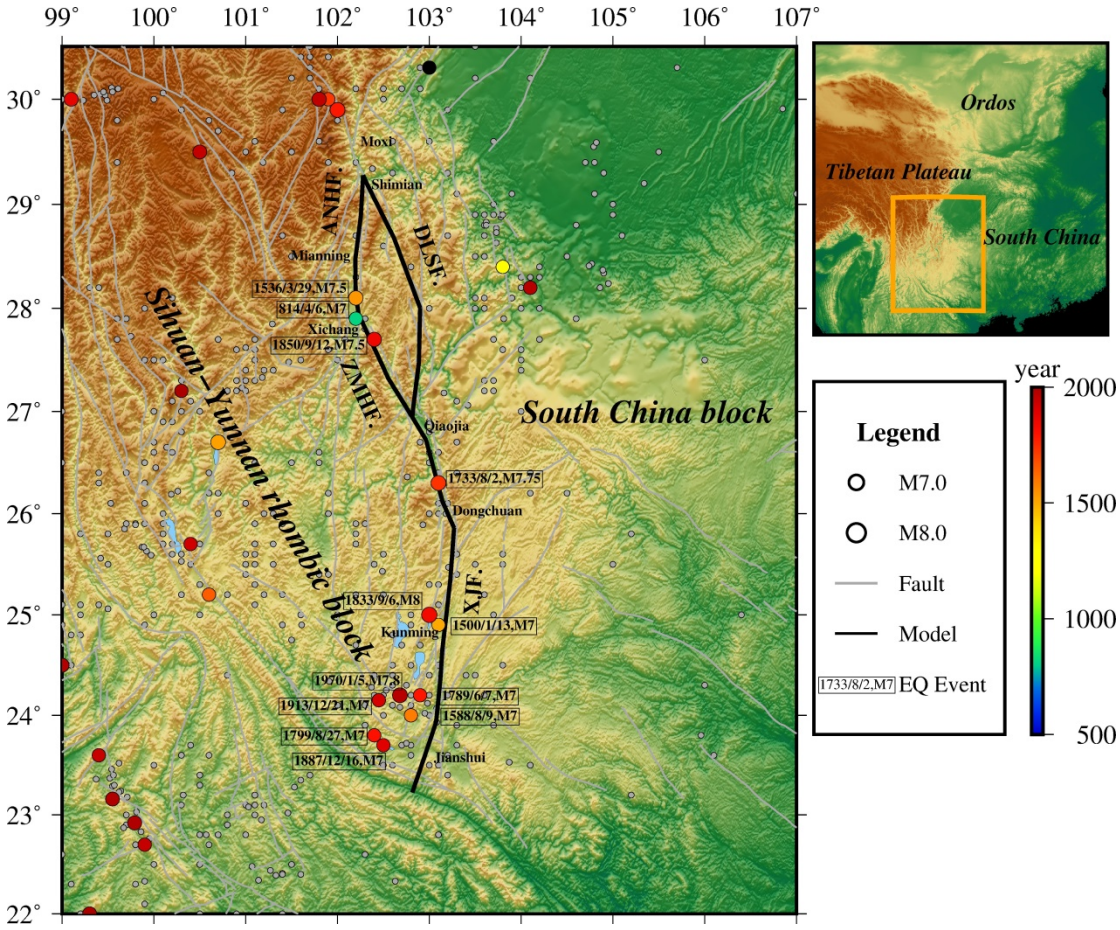

Figure 1. Tectonic and topographic map in the AZDX fault system and its surrounding regions. Fault abbreviation: ANHF., the Anninghe Fault; DLSF., the Daliangshan Fault; ZMHF., the Zemuhe Fault, XJF., the Xiaojiang Fault. Dark gray lines represent active faults (Deng *et al.*, 2003a), and black bold lines represent synthetic faults constructed in this study. Colored circles show historic strong earthquakes M 7; Dark gray show earthquakes magnitude from 5 to 7 (Department of Earthquake Disaster Prevention, 1999). Black rectangles include the earthquake event time and magnitude. Grey circles mark the historical earthquakes before 1970 and colored circles show earthquakes (M 7.0) between 500 and 2021.

In this study, we aim to simulate a long-term synthetic earthquake catalog in AZDX fault system, southwestern China, by applying the VQ. The 3-D fault model of the AZDX fault system is constructed and constrained by recent GPS and seismic observations. Then, the VQ earthquake simulator is applied in our study region to generate a long-term (20 thousand years) synthetic earthquake catalog. Such a long-term catalog can be used to characterize several statistics

of earthquakes and evaluate seismic hazard. Moreover, we discuss our results considering model uncertainties and future development.

1. **Methods of the physics-based earthquake simulation**

2.1 Virtual Quake Simulator

As a physical-based simulation model, VQ is formed by three major components: a fault model, a set of quasi-static elastic interaction between faults (governed by Okada's implementation of Green's functions (Okada, 1992)) and a rupture event model (Sachs *et al.*, 2012; Yoder *et al.*, 2015). In the fault model, faults with geometrical characteristic (strike, dip angles and depth) specified at each trace point are embedded in a flat homogeneous half-space. The estimated slip rates along a fixed rake vector, the aseismic slip and parameterization of friction laws based on laboratory experiments are also vital to assign on each trace points as the input. Then the fault planes are meshed into rectangle elements by setting an appropriate element size. The element size equals to the minimum simulated rupture area, governing the minimum magnitude of simulated earthquake.

Based on a geometrically static fault system assumption, faults don't move actually in the VQ model (Rundle *et al.*, 2012). Back slip model is applied to describe the effects of the stress buildup and release along the fault plane. Thus, for a ruptured element has slipped, the original position is identical to the equilibrium position. The relative position and orientation of each element that determines the interactions between faults is invariable. That indicates the Green's function matrix do not change once been calculated.

2.2 Rupture model

In the VQ simulator, the process of an event model accumulated or released stress consist of two parts: the long-term plate movement which can been described by fault slip rate and the rupture propagation (Sachs *et al.*, 2012). In addition, the rupture model consists of two internal phases: (1) slip caused by static or dynamic friction, (2) slip induced by the influence of other elements (interaction between elements). In the first stage, the Coulomb failure function (Stein, 2000) is employed to calculated element failures. The CFF is given by:

$$CFF(x,t) = \sigma_s(x,t) - \mu_s \sigma_n(x,t) \quad (1)$$

Where μ_s is the static friction coefficient, σ_s is the shear stress along the element rake vector and σ_n is the normal stress perpendicular to the element. When the stress loading exceed the threshold value ($CFF \geq 0$), the elements start the initial rupture and slip which defined as static failure. When significant change of CFF caused by stress increasing and satisfies the formula (2), dynamic failure proceeds. In the dynamic failure stage, ruptured elements continue to slip and propagate rupture to the elements physically nearby.

$$\frac{\mathrm{CFF}_{\mathrm{init}}(x,t) - \mathrm{CFF}_{\mathrm{final}}(x,t+t)}{\mathrm{CFF}_{\mathrm{init}}(x,t)} > \eta \quad (2)$$

Here, t can be interpreted as being the time since the beginning of the earth-

quake at time t. And the critical stress rate η, as a primary tuning parameter in the VQ model, defined the dynamic trigger factor which is used to control rupture propagation during a simulated earthquake, ranging from 0 to 1. Greater dynamic factor promotes earthquakes propagation and induces great earthquake with higher probability. When dynamic trigger factor $(\eta) = 0$, the entire fault is allowed to rupture together (Khodaverdian *et al.*, 2016a) .

Based on the rate-and-state and leaky threshold laws (Rundle and Klein, 1995), Rundle further generalize these friction laws to include two additional term as the Eq. (3) (Rundle *et al.*, 2006): the stable stress-dependent aseismic sliding (the first term in Eq.(3)) and the term depended on stress increase rate (the third term in Eq.(3)). And the stress drops σ for the element in the model is defined by Eq.(4).

$$\frac{\partial s}{\partial t} = \frac{\sigma}{K_T}\left\{\alpha + \delta\left(t - t_F\right) + \beta\delta\left(\frac{\partial \sigma}{\partial t} - \eta\right)\right\} \quad (3)$$

$$\frac{\sigma}{K_T} = \frac{\sigma(x,t) - (\mu_s - \mu_k)\sigma_n}{K_T} \quad (4)$$

Here σ is the stress drop, K_T is the total spring constant related with a fault segment, s is slip amount and the μ_k is kinetic friction coefficient. The t_F is the time at which $\sigma = \mu_s \sigma_n$. δ is the Dirac delta function. In the first term, the aseismic slip factor α is related to fault creep. Stable aseismic slide can occur with proportional to α for non-zero σ preceding the instability at $t = t_F$. The second and third term represent the unstable slip related to static and kinetic friction. In the second term, when $\mathrm{CFF}(x,t) = 0$, there exists unstable slip caused by static friction. Then stress increasing, unstable slip occurs by the kinetic friction under the condition of Eq. (2) as the third term shows.

As another critical tuning parameter such as dynamic trigger factor η, stress drops play a critical role in the simulation as well. On the basis of a large number of observations, Wells and Coppersmith (Wells and K. J. Coppersmith, 1994) present the empirical statistical relationships between magnitudes and fault rupture parameters which is the most widely used . Based on published empirical scale relations between the magnitudes and the rupture area (Hanks and Bakun, 2002; Somerville *et al.*, 1999; Wells and K. J. Coppersmith), Leonard (2010) proposes more detailed scaling relations which are self-consistent, including moment, rupture length, width, area and displacement to be estimated. According to Leonard (2010), when given a certain fault area, the predicted characteristic magnitude M, with assumption of the entire fault segment area ruptures to generate essentially same size earthquakes (Schwartz and K. J. Coppersmith, 1984), is characterized as:

$$M^{\mathrm{char}} = 4.0 + \log_{10}(A) + \ M \quad (5)$$

Here, A is the fault area in unit km^2, M is the stress drop factor value for adjusting the correlative characteristic stress drop, ranging from 0.2 to 0.8 typically. Once the characteristic earthquake magnitude is settled, the mean slip can be derived from the seismic moment definition (Kanamori and Anderson,

1975). Then the shear stress drop σ of given fault area in the elastic half space can be acquired employing the analytical solution. To facilitate understanding, the shear stress drop can be approximated as the proportional relation with fault geometry and slip amount (Wan, 2016):

$$\sigma \sim \frac{2\mu\, s}{W} \quad (6)$$

Here, s is the mean slip, as the function of fault area, stress drop factor and M^{char} , μ is the shear module, W is related to the characteristic rupture length. Increasing stress drop factor tends to increase global stress in a log scale. And greater earthquakes occur with the larger stress drop factor assigned. Through tuning stress drop factor and dynamic trigger factor, the frequency-magnitude relation of the simulated seismic catalog can match that of the actual seismic record.

Study on aftershock sequence and its physical mechanism is one of the important ways to comprehend seismic process. In addition to the physical-based rupture model, the probability model of aftershock sequences is taken into consideration in the VQ model as well. It has been known that the epidemic type aftershock model (Ogata), following the similar rate with the magnitude of the father earthquake, has been widely used to practice in earthquake forecasting and seismicity analysis. Based upon ETAS model, Turcotte *et al.* (2007) proposes the Branching Aftershock Sequence model, whose sequential time, space and intensity distribution completely self-similar. To better describe the trigger and attenuation of aftershocks, VQ introduces the BASS model as the aftershock model.

1. **Parameters of simulations**

3.1 Fault model of the AZDX fault system

Constrained by the previous studies (Deng *et al.*, 2003b; He and Oguchi, 2008; Song and Wang, 1998), the fault trace along the surface is simplified for the fault model (Figure 2). Referring to the fault locking depth (Li *et al.*, 2014; Wang *et al.*, 2011b) and fault model constructed in previous study (Jiang *et al.*, 2015b), the fault depth is extended to 20 km. We assume fault plane to be upright (dip=90°) to the surface, mainly based on the following considerations: (1) fault planes in the AZDX fault zone are almost vertically dipping (He and Oguchi, 2008; Jiang *et al.*, 2015a; Song and Wang, 1998); (2) the behavior of the AZDX fault is dominated by strike slip (He and Oguchi, 2008; Jiang *et al.*, 2015b; Song and Wang, 1998) and the dipping slips far less than the striking slips which indicates dipping slips can be dismissed; (3) The interaction between elements mainly depends on the distance between the elements. When the dip angle of the fault plane changes, the relative distance between the elements does not change much, and it effect negligibly on the corresponding interaction. Meanwhile, we set the rake angle 0°which means pure left-lateral strike slip based upon the second consideration. The Lame parameter, mu (μ) and lambda (λ), describing material properties can be derived from the wave velocity (V_p and

V_s) and the density (ρ). The aseismic and evaluated fault slip rate are further discussed in the next section.

After all the fault geometry characteristics are assigned, the fault plane is discretized into rectangle segments with same element size we set. In the VQ model, minimum magnitude depends on the slip distance and element area. When the element size increases, the minimum event magnitude increases logarithmically, and the total number of elements in a model decreases. Accordingly, more memory requirements are needed. Linear interpolation is used for meshing the fault plane into same size element. When the residual length after meshed is less than the element size, the fault plane will be lengthened to satisfy the element size. In consideration of the computational efficiency and the minimum event magnitude, we set the element size to be 3 km. Hence there exist 7 elements along the depth which suggests the actual depth of the fault model is 21 km (Figure 2). All the parameters are shown in the table 2.

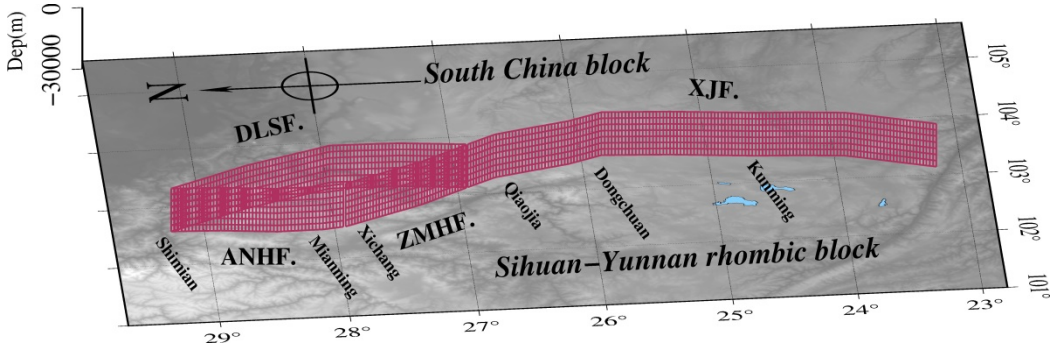

Figure 2. Three dimensional model of the AZDX fault plane. The dark red rectangle represents the element with 3km×3km size. Fault abbreviation: ANHF., the Anninghe Fault; DLSF., the Daliangshan Fault; ZMHF., the Zemuhe Fault, XJF., the Xiaojiang Fault.

Table 1
Mechanical Properties of AZDX fault model.

Parameters	**Value**
Simulated period	,000 years
Element Size	km
Stress Drop Factor	
Dynamic Factor	
Lame's mu (μ)	3.27e+10 Pa
Lame's lambda (λ)	3.27e+10 Pa
Aseismic Slip	

1. Fault slip rates

In the past decades, the Holocene and present-day slip rates of the AZDX fault system by means of geological (Chen and Li, 1988; He and Oguchi, 2008; Ran *et al.*, 2008b; Sun *et al.*, 2015; Wei *et al.*, 2012; Xu *et al.*, 2003) and geodetic studies (Jiang *et al.*, 2015b; Li *et al.*, 2021; Shen *et al.*, 2005) within the acceptable difference range have been published. Li *et al.* (2021) reported the updated fault slip rates inferred from the linear spherical block model based on the recent geodetic observation. Their results, describing the long-term relative micro-plate motions, can represent the long-term fault slip rate of the AZDX fault (Li *et al.*, 2021). The fault slip rates exhibit consistency with previous geological estimates and the geodetic studies which detailed comparison is included in the supplementary material of Li *et al.* (2021). Therefore, we use their slip rates in our simulation to obtain a long-term seismic catalog of the AZDX fault system. The fault slip rates are displayed by different colors in the Figure 3, and are summarized in the Table 2.

The aseismic parameter of the VQ simulator, referring to the creep portion of total fault slip, is treated to enhance the verisimilitude of simulation (Rundle *et al.*, 2001). In the AZDX fault zone, there's no explicit quantification of aseismic fault slip. Given as the eastern boundary of the Tibetan extrusion tectonics (Tapponnier *et al.*, 1982), the AZDX fault zone is the most seismically active deformation zone in southeastern China. Considering the high seismicity of the AZDX fault zone, aseismic slip can be neglected in this model.

Table 2
Fault Slip Rates of the AZDX fault model.

Fault Name	**Slip Rate (mm/yr)** *
Anninghe Fault	~7.6 (LL)
Zemuhe Fault	~6.6 (LL)
Daliangshan Fault	~5.9 (LL)
Xiaojiang Fault	~13.8 (LL)

*LL, left-lateral

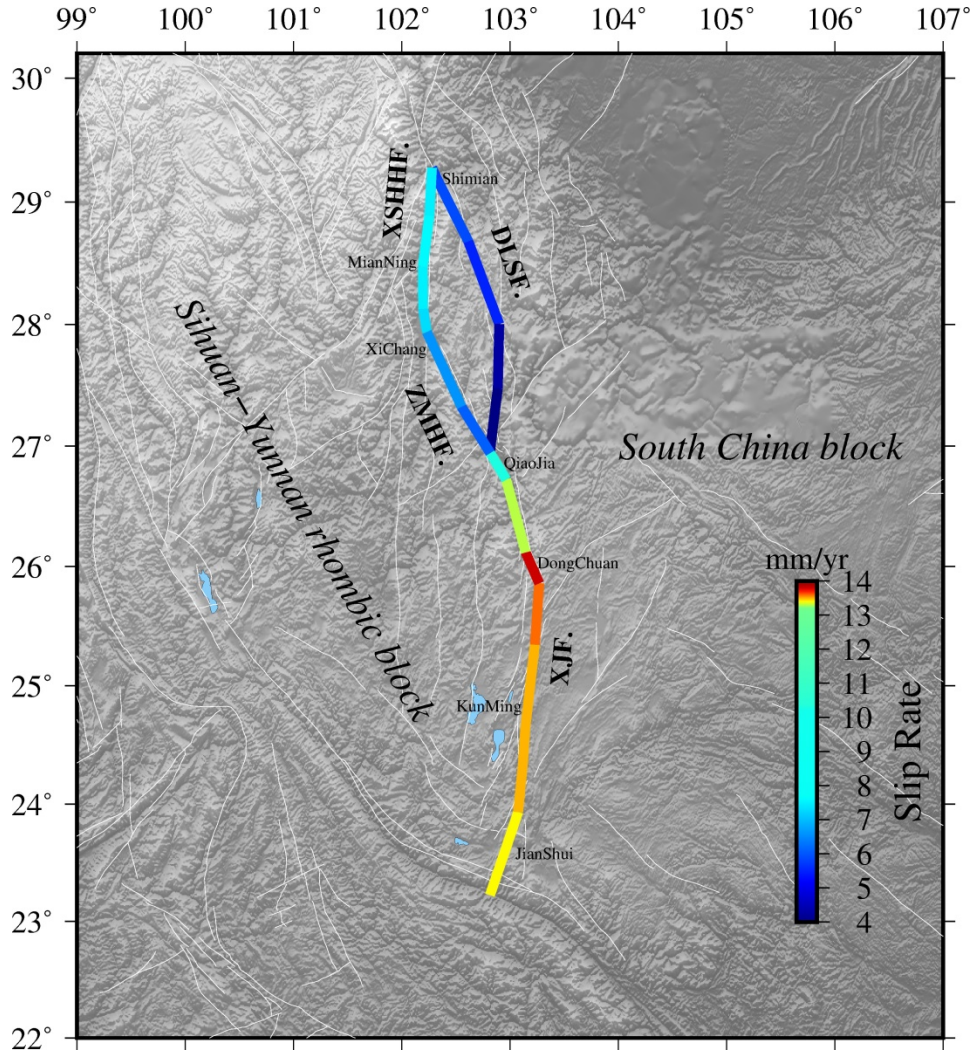

Figure 3 Slip rates of the AZDX faults. The value represented by the color corresponding to the color scale is the fault left-lateral strike-slip rate value. Fault abbreviation: ANHF., the Anninghe Fault; DLSF., the Daliangshan Fault; ZMHF., the Zemuhe Fault, XJF., the Xiaojiang Fault.

3.3 The G-R relation of the historical seismic catalog

The frictional physics of earthquakes leads to self-organization of statistical dynamic and produces statistical distribution similar to the observed events in nature (Rundle *et al.*, 2004), particularly obeying the Gutenberg-Richter law, which stated the earthquakes number $N(m)$ with magnitude m described in the Eq. (9). Therefore, the synthetic seismic catalog can be employed to match the G-R relation of historical seismic catalog for model verification.

$$\log_{10} N(m) = a - bM \quad (9)$$

Here, b value is the slope of the frequency-magnitude relation.

However, due to the relatively short period of modern observation of earthquakes, there is no a relatively complete and unified regional seismic catalog in Sichuan-Yunnan region. We aim to make full use of available observed seismic catalog and estimate a reasonable completeness magnitude M_c to ensure the integrity of catalog. The historical seismic catalog with a time span from the 23^{rd} century B.C. to 1990 with magnitude above M4.7 has been compiled by the Department of Earthquake Disaster Prevention, China Earthquake Administration (Department of Earthquake Disaster Prevention, 1995). From the historical seismic catalog by CEA and the China Earthquake Networks Center (CENC), the observed catalog (M 4) of AZDX fault zone is gathered whose time span ranges from 647 to 2021. The frequency-magnitude distribution of this seismic catalog with magnitude interval of 0.1 is shown in the Figure 4.

When the G-R relation can be best fitted to cumulative frequency-magnitude distribution, the corresponding minimum initial magnitude is defined as the completeness magnitude. In accordance with the definition, the completeness magnitude can be rough estimated by the G-R curve in Figure 4. The Figure 4 exhibits the significant characteristic of the b-value, which varies greatly at M=5. The b-value of magnitude less than M5 is 0.1 with flat curve. But the curve becomes steep notably when the magnitude above M5 with the b-value of 0.66. Accordingly, the completeness magnitude of the historical seismic catalog in AZDX fault zone is regarded as 5.0. The G-R relation of the historical catalog larger than the M_c is available for the validation in the model parameter choice.

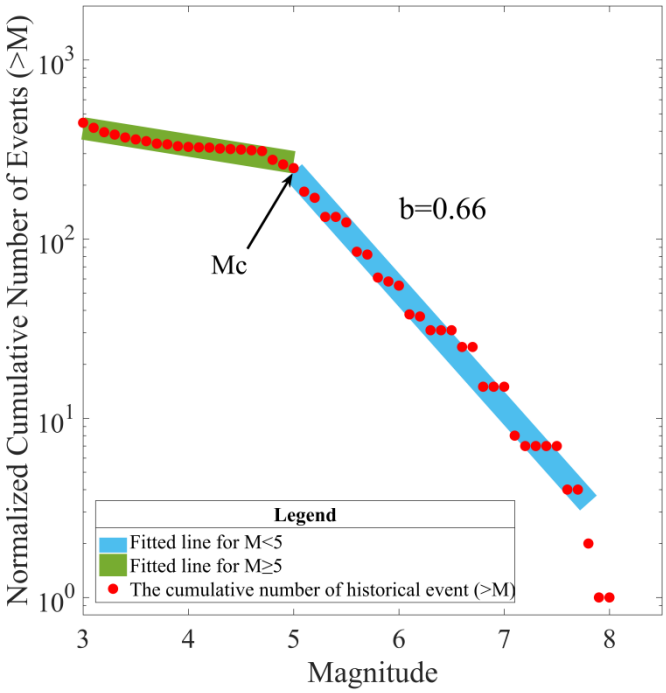

Figure 4 The cumulative frequency-magnitude distribution of historical seismic catalog with M 3 in the AZDX fault zone. Red dot: the cumulative number of events; Green shadow: fitting line of the catalog with 3 M 5; Blue shadow: fitting line of the catalog with M 3. The magnitude interval is 0.1.

1. Choices of model parameter

Two critical tuning parameters, the stress drop factor M and dynamic trigger factor η delineated in section 2.2, can affect simulated earthquake magnitude and propagation. In this section, we chose the two parameters for matching the frequency magnitude of the synthetic seismic catalog to the G-R relation of observed catalog for model validation. In the VQ simulator, the stress drop factor, not directly equivalent to the stress drop defined in the rate and state dependent friction laws, essentially is an empirical parameter tuning scale relations between magnitude and rupture area ($M \sim A$). Larger values of stress drop factor tend to generate large earthquakes with long period. Accordingly, the low strain regions yield to low stress drop factor. In mid-continental crust and stable continental regions, the stress drop factor at 0.3~0.4 accounts for an assumed higher stress drop fittingly (Somerville *et al.*, 1999). For modeling the eastern part of the Iranian plateau characterized by large and infrequent earthquakes, the stress drop factor value of 0.3 is consistent with actual earthquake rates (Khodaverdian *et al.*, 2016a). In the California model (Rundle *et*

al., 2006), which is a large shear zone with complex faults system, stress drop factor value is restricted within a certain range of 0.6~0.8. For the model of AZDX faults zone dominated by remarkable left lateral strike slip with simple fault system, reasonable stress drop factor value should be selected from 0.5 to 0.7. Furthermore, we estimate the range of the dynamic trigger factor value based on the empirical value (Khodaverdian *et al*, 2016; Rundle *et al.*, 2006). Here, in the AZDX model, dynamic trigger factor value limited in 0.7, 0.8 and 0.9 is assigned to experiment with fixing stress drop factor value at 0.5, 0.6 and 0.7, respectively. Conclusively, the combination values of dynamic trigger factor and stress drop factor are at 0.8 and 0.6 individually.

Assigning different combinations of stress drop factors and dynamic trigger factors to the AZDX model, we compare the corresponding frequency magnitude distributions with the G-R relation of historical seismic catalog (Figure 8). The final two tuning parameters ($\eta = 0.8,\ M = 0.6$) which suit the observed catalog appropriately are determined for the AZDX model. More details of choices of those two parameters and discussion of uncertainties on simulated results can be found in section 5.1.

1. **Simulation results**

We simulate a 20,000 years of synthetic seismic catalog on the basis of present fault behavior by applying the VQ. The synthetic seismic catalog has been provided on the supplementary material. In this section, we analyze the spatiotemporal feature of this synthetic seismic catalog, especially the strong earthquakes occurrence rate and the recurrence interval for evaluating the seismic hazard risk of the AZDX fault system.

1. Seismic rates and recurrence intervals of the AZDX faults

The seismic rates of strong earthquakes (M 7), which denote the numbers of strong earthquake per year in a specific fault, is characterized to show the spatial distribution of the simulated seismic catalog. Because different parts of faults may behave differently in terms of slip rates and geometries, seismicity in difference sections of faults may vary accordingly. Give consideration to that, the occurrence intervals of strong earthquakes are specified by sections in this study. According to the empirical relationship between strike-slip rupture length (L) and co-seismic displacement ($\log_{10} D = -0.72 + 0.72 \log_{10} L$), as well as the empirical relationship between earthquake magnitude and co-seismic displacement ($M = 5.1 + \log_{10} L + \log_{10} D$) derived by Deng *et al.* (Deng *et al.*), we can roughly estimate that the surface rupture length corresponding to a M7 earthquake is about 30 km. Therefore, splitting the fault trace into sections with 30km is reasonable (Figures 5 and Table 4). In each section, we sum up the numbers of the earthquakes with M 7 occurring in all depths, and signifies them with the color scale as shown in the Figure 5a. Accordingly, all the value of the strong earthquake occurrence rate (total and annual) in each section is listed in the Table 3.

As shown in the Figure 5a and the Table 3, we acquire the characteristics that

the sections with large occurrence rates are mainly concentrated in the middle and the southernmost sections of the Xiaojiang fault. Remarkably, the southernmost section (390~426km) of the Xiaojiang fault is the largest strong earthquake occurrence rate area where exists 32 strong earthquakes (M 7). For the Anninghe-Zemuhe fault, more strong earthquakes are located in the northern section of Anninghe fault (0~60km). All sections of the Anninghe fault, the middle-southern sections of Daliangshan fault (60~270km) and the northern sections of Xiaojiang fault (0~90km) are with relatively less strong earthquakes (10) generated in the simulation. The strong earthquake occurrence rate of the Daliangshan fault, excluding that of the northern sections (0~60km), exhibits a low level (5), especially the southernmost section with no strong earthquakes.

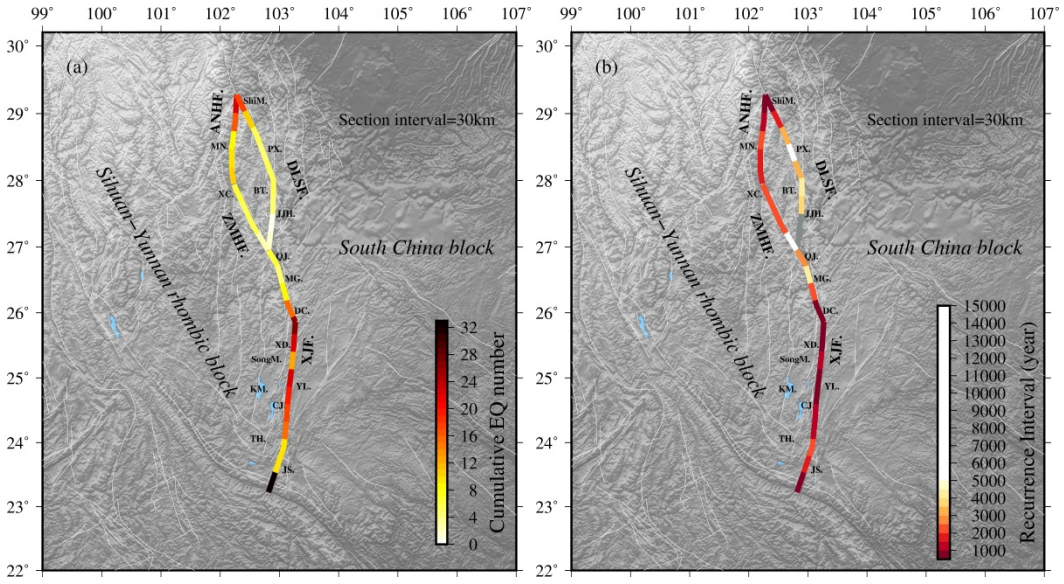

Figure 5 (a): The cumulative numbers of simulated strong earthquakes (M 7) in each section with 30km interval of the AZDX faults. Different numbers in each separated fault section is represented by different colors. (b): The mean recurrence intervals of strong earthquakes (M 7) in each section. Mean recurrence rates in each separated fault trace characterized by color scale correspond to the color scale. Gray color signifies lack of recurrence interval. Fault abbreviation: ANHF., the Anninghe Fault; DLSF., the Daliangshan Fault; ZMHF., the Zemuhe Fault, XJF., the Xiaojiang Fault. City abbreviation: ShiM.: ShiMian; MN: MianNing; PX: PuXiong; XC: XiChang; BT: BuTuo; JJH: JiaoJiHe; QJ: QiaoJia; MG: MengGu; DC: DongChuan; XD: XunDian; SongM: SongMing; KM: KunMing; YL:YiLiang; CJ: ChengJiang; TH: TongHai; JS: JianShui.

According to the occurrence rates of strong earthquakes (M 7) with 30km interval given in Figure 5a, we obtain the mean strong seismic recurrence interval within 20 thousand years on each section by equation (10) and display it in Figure 5b.

$$R = \frac{T_{\text{last}} - T_{\text{first}}}{N-1} \quad (10)$$

Here, R is the mean seismic recurrence interval. N is the number of earthquakes in the specified section which is listed in the fourth column of Table 3. And T_{last} and T_{first} are the occurrence time of the last and first strong earthquake, respectively.

The Figure 5b reveals the spatial feature of mean seismic recurrence interval in different sections. In contrast to Figure 5a, deeper color represents shorter strong seismic recurrence interval of each section. The mean recurrence interval of the Anninghe fault ranges from 911a to 2294a, and only that of 60-90 km section is more than 2ka. The whole Zemuhe fault behaves with a long recurrence interval (2.1ka). With the exception of the northern part with a recurrence interval shorter than 2ka, the occurrence interval of the Daliangshan fault is more than 3ka.

Due to the insufficiency of strong earthquakes number in the end two sections, the mean strong seismic recurrence interval can't be provided. Nevertheless, it implies that the strong earthquakes in the end sections of Daliangshan fault may recurred with a long recurrence interval (20ka). Strong earthquakes recur with a short interval (1ka) in the northernmost (near Shimian) and southernmost sections (south of Jianshui) of the fault model. The end section is prone mostly to stress accumulation relative to other section, and the slip rate of the end section is not pinched out. Therefore, we cannot rule out that this is due to end effects. The Figure 5b also indicates that the Xiaojiang fault is characterized with segmentation: 1. From the northern part to the middle part, there's a notable trend that the strong seismic recurrence interval gradually shortens; 2. Most sections of the middle part show strong seismic recurrence interval more than 1ka; 3. In southern part, except for the end section (390~426 km), strong earthquakes on other sections recur with period greater than 1ka. As the deep red color signifying, the most active region of the AZDX fault system is the section near the south of Dongchuan with recurrence interval of 600~800 a.

Through the mean strong seismic recurrence interval and occurrence rate on different sections, we summarize the segmented feature of simulated catalog that the high-seismicity sections with relatively short strong seismic recurrence interval (1ka) distribute mainly in the northern part of the Anninghe fault, the middle part and the end part of the Xiaojiang fault are. Whereas, the strong earthquakes recurrence with a relative long period (>3ka) in the middle-southern part of the Daliangshan fault and the end part of the Zemuhe fault.

Table 3

The occurrence rates and mean recurrence intervals of strong earthquakes (M 7) in the simulated seismic catalog on each section of the AZDX faults.

Fault Name	Section Name	Section(km)	Occurrence Rate	Occurrence Rate(yr^{-1})	Recurrence Interval(years)	Latest Events M 7	References
ANHF.	Northern Section (Shimian-Mianning)	~30		1.1E-03			
		~60		9.2E-04		M7.5±0.3	(Wen *et al.*, 2000)
		~90		5.0E-04			
	Southern Section (Mianning-Xichang)	~120		5.3E-04			
		~147		5.9E-04		M7 1536 M7½	(Department of Earthquake Disaster Prevention, 1995; Ran *et al.*, 2008a)
ZMHF.		~30		5.4E-04		,M7½	(Wen, 1993)
		~60		5.7E-04			
		~90		5.0E-04			
		~123		1.4E-04			
DLSF.	Shimian-Yuexi	~30		1.1E-03		3500aBP	(Song *et al.*, 2002)
		~60		6.3E-04			

Fault Name	Section Name	Section(km)	Occurrence Rate	Occurrence Rate(yr^{-1})	Recurrence Interval(years)	Latest Events M 7	References
	Puxiong	~90		3.8E-04		24000aBP(8050±240aBP	(Xiao *et al.*, 2016; Song *et al.*, 2002)
		~120		2.6E-04			
		~150		3.8E-04			
	Butuo	~180		2.9E-04		7500aBP	(Song *et al.*, 2002)
		~210		3.5E-04			
	Jiaojihe	~240		-	-	4500aBP	(Song *et al.*, 2002)
		~270		-	-		
XJF.	Northern Section (Qiaojia-Menggu)	~30		4.7E-04			
		~60		3.1E-04			
	Middle Section (Dongchuan)	~90		5.3E-04		Dongchuan M7.75	(Department of Earthquake Disaster Prevention, China Earthquake Administration, 1999)

Fault Name	Section Name	Section(km)	Occurrence Rate	Occurrence Rate(yr^{-1})	Recurrence Interval(years)	Latest Events M 7	References
		~120		1.1E-03			
	Middle Section (Xundian)	~150		1.6E-03			
		~180		1.4E-03			
	Middle Section (Songming)	~210		8.9E-04		Songming M8.0	(Department of Earthquake Disaster Prevention, 1999)
	Middle Section (Yiliang)	~240		2.1E-03		Yiliang M7¾	(Shen and Wang, 1999)
		~270		1.1E-03			
	Southern Section	~300		9.5E-04		Huaning M7	(Mao, 2001)
		~330		8.4E-04			
		~360		4.9E-04			
		~390		5.8E-04		Jianshui M7.23~7.6	(Mao, 2001)
		~426		1.7E-03			

Upon the Chinese strong seismic catalog, the earliest recorded of Chinese earthquakes can backtrack to the 23rd century B.C. (Department of Earthquake Disaster Prevention, 1995 1995). However, there are only 15 determinate earthquake records before Common Era. Besides, large amount of doubtful material and earthquakes with unascertainable epicenters exist. Simply employing the histor-

ical earthquakes records for comparison with strong seismic recurrence interval of the synthetic seismic catalog seems deficient.

Paleoseismic investigations play an important role in detecting fault segmentation and paleoearthquakes recurrence interval, and period of the latest earthquake on individual Quaternary faults (Crone and Haller, 1991; Schwartz and K. J. Coppersmith, 1984) and supplementing the seismic catalog. Previous researchers have conducted catalogs on the rupture relics of historical earthquakes and paleoearthquakes in the AZDX region. By recognition of preserved geological evidence of paleoearthquakes occurred on active faults, the approximation of paleoearthquake recurrence interval with long timescale will be revealed. However, in the absence of event dislocation, slip rates and other data, the paleoearthquake magnitude can't be identified. And it has been recognized that earthquakes less than M7 can also generate rupture on surface and be marked in the geological record (Li *et al.*, 2018; Xu *et al.*, 2015; Song *et al.*, 1998). That is to say that not all estimated recurrence interval by paleoearthquakes are related to M7 or above. In this paper, we only concern on the strong earthquakes with magnitude equal to or greater than M7. For the paleoearthquakes, without approximate magnitude but given the rupture area or length, we can estimate via empirical scaling relations such as the commonly applied WC94 (Wells and K. J. Coppersmith, 1994).

ANHF

Northern part

Due to human being underdevelopment and remoteness location, the northern part of the Anninghe fault (Shimian-Mianning) lacks seismic records before 1910, and only one destructive earthquake of magnitude 6 was recorded until 1913 (Wen *et al.*, 2000). However, some paleoseismic studies have been carried out along the northern part of the Anninghe fault. Four paleoseismic events with mean magnitude of M7 preliminarily indicate that paleoearthquakes occurred with roughly similar intervals of 940±150a (Qian, 1992). In accordance with the calculation of the horizontal displacement of 3~4 m, the mean recurrence interval of strong earthquakes is about 670~890a (Wang *et al.*, 2013). Applying the empirical scaling relation between the co-seismic displacement and the moment magnitude (WC94), we estimate the moment magnitude of paleoseismic events with 3~4 m horizontal displacement is about M7.5. In that case, the recurrence interval of the M7.0 should theoretically be less than 670~890a. Similarly, on the basis of new insights proposed by Ran (Ran *et al.*, 2008a) the recurrence interval of M7.0 is less 520~660a. By contrast, the simulated strong recurrence interval of 911~2294a in the northern part (0~90 km) includes the recurrence interval obtained by Qian *et al.* (1992).

Southern part

Ran *et al.* (2008) conclude that the Anninghe fault is segmented in Mianning area with relatively independent strong earthquake rupture history in the south and north. However, the paleoseismic research degree in the southern part of

Anninghe fault is low. Referring to Wang (Wang, 2013), we reckon that the recurrence interval of M7.0 is less than 1400±170a via the WC94 scale relation. In the sections of 90~120 km and 120~147 km, the simulated mean recurrence interval are 1608a and 1559a, within the reasonable range speculated by paleoearthquakes. According to the historical materials, the epicenters of earthquakes with magnitude above M7, occurring in 817 and 1536 respectively, are geographically closed, and the interval between the two earthquakes was 719a, which was much lower than the mean interval of the simulation (1559~1608a).

ZMHF:

The study of earthquake-caused landforms indicates the recurrence characteristic. By the field investigations and C^{14} data, Ren *et al.* (1989) presents that the northern Zemuhe fault has experienced at least four strong earthquakes since the late Pleistocene and calculated the minimum recurrence interval of earthquakes with M7.0 or above is 1000a, and the mean interval is 1800a. Based on the further research on landforms and exploratory trench, Ren *et al.* (2007) conclude three paleoseismic events and obtains the recurrence interval of strong earthquakes whose magnitude equivalent to the magnitude of 1850 Xichang M7.5, is 2300 3000a in northern part. Xu and Deng (1996) ascertains the longest recurrence interval for paleoearthquake is 6.2ka, and the shortest is 1036a with four earthquakes (M 7) identified in the Holocene along the northern part.

The recurrence interval of strong earthquakes (M 7.0) of the synthetic seismic catalog in the middle-northern sections (0~90 km), about 2.2ka, is closed to that estimated by Ren *et al.* (1989, 2007) and within the range of Xu and Deng (1996). Obviously contrasting with the northern Zemuhe fault, no evidence available for surface rupture during the Holocene observed along the south (Xu *et al.*, 1996), and no historical earthquakes (M 7) are recorded, as well. Only two strong earthquakes are simulated in the end section (90~123 km) with an interval of 10 thousand years scale which illustrates inactive seismicity in this section.

DLSF:

Detailed studies for a long period on the new active characteristics of Xianshuihe-Xiaojiang fault zone, the relationship between faults and strong earthquakes, and the paleoearthquakes have been achieved. Abundant research conclusions have been attained for the Xianshuihe-Xiaojiang fault zone, but the Daliangshan fault zone doesn't draw enough attention. The economy and culture of the area where Daliangshan fault zone located is relatively underdeveloped, so historical earthquakes of M6 or above have not been recorded. However, the Daliangshan fault zone possesses the geological conditions for earthquakes with M7 or above which has been revealed by excavating exploratory trenches (Song *et al.*, 2002; Sun *et al.*, 2019a). In the exploratory trench near the Shimian, two paleoearthquakes with recurrence interval of 10 thousand scales are discovered by Song *et al.* (Song *et al.*, 2002) and Sun *et al.* (2015). Sun *et al.* (2015) insists that there may be seismic events not recorded in this trench and further pale-

oseismic studies should be conducted. For corresponding section (0~30 km) in the fault model, the strong seismic recurrence interval averaged by 17 synthetic earthquakes is less than 1ka.

In the middle section of Daliangshan fault, two paleoseismic events, which occurred in 730±160a BP and 3050±240a BP individually, have been revealed in near Puxiong (Gao *et al.*, 2016). Of the two paleoearthquakes, only the magnitude of second last event has been confirmed above M7. In the related section (90~120 km), the simulated recurrence interval is 3267~5199a. Even the magnitude of latest paleoseismic is above M7, the simulated recurrence interval is larger than that derived by paleoearthquakes.

For the recurrence intervals in southern sections, researchers carry out different results. According to the exploratory trench in the north of Butuo, Song *et al.* (2002) discovered three paleoearthquakes which the recurrence interval of last two paleoearthquakes is 2.5ka. And we get a strong earthquakes recurrence interval of 3795~4244a which is larger than that derived by the two paleoearthquakes. In the south of Jiaojihe, Song *et al.* (2002) summarizes the recurrence interval of two paleoearthquakes is 4.5ka. But He *et al.* (2008) revealed the last paleoseismic event occurred about 1520~1950a ago by exploratory trench. This means that the recurrence interval may be larger than 1520~1950a in the adjacent area of Jiaojihe. By dividing average slip rate with co-seismic displacement of three paleoseismic events, Wei *et al.* (2012) obtained that the mean paleoseismic recurrence interval is about 2ka. But He *et al.* (2008) and Wei *et al.* (2012) don't provide the approximation of paleoseismic magnitude. Therefore, we can't summarize a relative uniform recurrence interval of M7 in the south section of Daliangshan fault. From the Figure 6(b) and Table 3, there exists only one simulated earthquake above M7 in the end two sections (210~270 km) which suggests the southernmost of Daliangshan fault is very inactive with recurrence interval of strong earthquake (M 7) up to 10ka.

Along the Daliangshan fault, the recurrence interval of paleoseismic events verified by exploratory trenches is almost larger than 2ka. However, few paleoearthquakes recur in situ are ascertained. We can't exclude the possibility of recurring aperiodicity and record lack, so recurrence interval summarized by small two paleoearthquakes may be partial. According to the distribution of mean recurrence interval acquired from the simulated seismic catalog (Figure 6(b) and Table 3), we summarize that the short recurrence interval locating in the north sections of Daliangshan fault and the long recurrence interval mainly spreading in the middle-south part. Except the beginning section (0~30 km) and the end 2 sections (210~270 km), the M7 or above recur with an interval of more than 2ka. Overall, there is a risk of earthquakes M7 or above in the Daliangshan fault but with a larger recurrence interval than that in the Anninghe fault and Zemuhe fault.

XJF

Referring to the studies on the fault internal structure, the Xiaojiang fault is

divided into three segments by Menggu and Chengjiang (Shen *et al.*, 2003; Song and Wang, 1998). The middle section, from southern Menggu to Chengjiang, consists of two branches, east and west. For simplification, the two branches are unified as one in fault model. Therefore, we don't distinguish west and east branches in the following discussion. Due to the frequent historical seismic activity in the north and middle sections of Xiaojiang fault, previous studies (Li *et al.*, 2018; Shen *et al.*, 2003 2003; Song and Wang, 1998) mainly focused on the middle sections. The southern segment of the Xiaojiang fault exhibits weak seismic activity in late Quaternary and no geological evidence of activity since late Pleistocene was found (Song and Wang, 1998; Wen, 1993). However, researchers (Mao, 2001; Wen *et al.*, 2008b; Zhao *et al.*, 2015) have indicated that potential seismic risk exists in the southern Xiaojiang fault using different methods.

Through analysis of geological and geomorphological phenomena with age, Chen *et al.* (1988) obtain the mean interval of M7~8 earthquakes recurring in situ is about 900a in the west branch of Xiaojiang fault and the mean recurrence interval of the whole Xiaojiang fault is about 300a. Except for the section of 60~90 km in the middle part, the mean recurrence intervals of other sections are approximately 894a, approaching that of west branch. In the Dongchuan section (60~120km) and Xundian section (120~180 km), Shen *et al.* (1998) estimates the mean recurrence intervals of earthquakes M 7 is about 200~500a and 300~800a, respectively. Between Dongchuan and Xundian, Li *et al.* (2018) also revealed seven paleoseismic events by exploratory trenches. Among them, last four paleoseismic events with continuous recorded suggest that the mean recurrence interval is about 370~440a. Although this actual mean recurrence interval matches well with that concluded by Shen, only the magnitude of last two events has been determined to be more than M7. According to the simulated seismic catalog, we note that the mean recurrence intervals of the corresponding sections of 60~120 km and 120~180 km are about 944~2158a and 643~764a, individually. The simulated mean recurrence interval of the Xundian section (120~180 km) is included in the range of actual mean recurrence interval, 300~800a. The simulated mean recurrence interval of southern Dongchuan section (90~120 km), 944a, coincides with that concluded by Chen *et al.* (1988). From the M7¾ recurrence interval of southern Dongchuan section laid out by Song *et al.*(1998), we speculate the M7 recurrence interval should be slightly less than 919~1837 a. According to geological mean recurrence interval for the whole middle section of Xiaojiang fault (Chen and Li, 1988), the simulated recurrence interval of M7, 944a, is appropriate. What's noteworthy is that the mean recurrence interval of the northern Dongchuan section (60~90 km) is greater than 2ka and is quite different from that of the southern Dongchuan section (90~120 km). It seems that the mean recurrence interval of the first three sections (0~120 km) has the same characteristics of more than 2ka.

The largest earthquake in the AZDX fault zone, the 1833 Songming earthquake of M8, occurred in the Songming section (180~210 km). The mean recurrence interval we obtained is 1226a and noticeably larger than the 764a on Xundian

section (150~180km) and 511a on Yiliang section (210~240 km). Nevertheless, Shen *et al.* (1998, 1999) infer that the recurrence interval of the M7±0.3 earthquakes near the epicenter of the 1833 Songming earthquake (M8) is about 300~800a. Song *et al.* (1998) concludes that the mean recurrence interval of M8 on the Songming rupture zone is 1073~2097 a. In the southern segment of the middle Xiaojiang fault, the Yiliang section (210~270 km), the simulated recurrence interval of M7 is about 511~972a which differs from 130~222a calculated with annual cumulative dislocations (Cheng *et al.*, 2011) and 2~3ka derived from trenches (Shen *et al.*, 2003).

Attributable to the neglect of its activity, the geological landform investigation and paleoseismological research in the southern part of Xiaojiang fault are still deficient. Derived from the M7.5 recurrence interval, 330~556a (Cheng *et al.*, 2011), the strong recurrence interval of earthquakes equal to 7.0 or large is supposed to be below 556a. We assess that the recurrence interval in the section of 270~390 km is more than 1ka. Significant contrast with the section of 270~390 km, the recurrence interval in the section of 390~426 km is 603a which may be due to the boundary effect.

1. **Probabilities of occurrence intervals**

As stated in previous section, the occurrence rate and mean recurrence interval strong earthquakes (M7) of each sections on the AZDX faults have been given. In most sections, the recurrence intervals of strong earthquakes (M7) occurred in the same section coincide well with that revealed by paleoearthquakes. Actually, the interaction between adjacent faults induces earthquakes swarm in same fault. Alternatively, recovery period after strong earthquake lasts for a long time exceeding the recurrence interval. In other words, strong seismic recurrence interval may be not quasi-periodic in a strict sense.

In this section, we count the intervals between two successive strong earthquakes of each fault and obtain the probability of occurrence interval (Figure 6). Considering the long extension of the Xiaojiang fault and its obvious segmentation characteristics, the Xiaojiang fault is divided into three segments for statistics. As shown in the Figure 6, our main conclusions are summarized as following:

1. Occurrence intervals between successive strong earthquakes range with a long period span. Such as the northern segment of Xiaojiang fault (Figure 6c) and Zemuhe fault (Figure 6f), the intervals extent of adjacent strong earthquakes covers from hundreds to thousands of years, and that of other faults also extend to thousands of years. This explains why the mean recurrence period of strong earthquakes varies greatly between adjacent sections on the same fault.

2. The recurrence intervals of the Anninghe fault (Figure 6a), Daliangshan fault (Figure 6b), middle and southern Xiaojiang fault (Figure 6d and 6e) occupies great portion in the section of 100~400a. The recurrence intervals of the Zemuhe fault hold a significant proportion in 200~1000a. In contrast, recurrence intervals of the northern Xiaojiang fault spreads distribute dispersedly.

3. As mentioned above, the seismic recurrence interval on the Xiaojiang fault appears segmental features distinguishingly for the northern section and south-middle section. For the middle section and south section of Xiaojiang fault (Figure 6d and 6e), the intervals of 200 years account for the largest proportion, which also indicates frequent seismic activity in the middle and south part of Xiaojiang fault. However, there's no notable difference in slip rate between the northern and the south-middle part but there is a visible difference on the fault strike. Thus, we hypothesized that the differences of recurrence intervals in different sections might be induced by the fault geometry. The specific influencing factors still need further work.

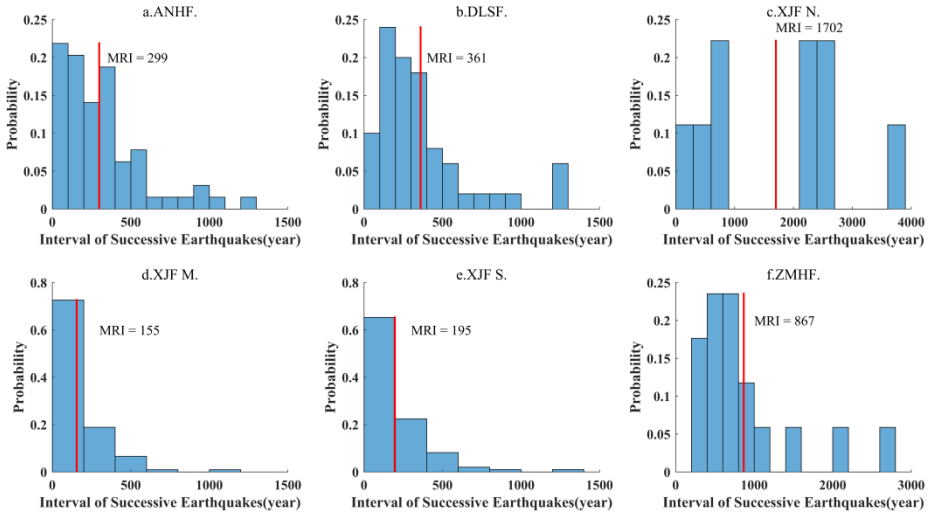

Figure 6 The probability of occurrence intervals of strong earthquakes (M 7) on each fault. Red lines show the mean recurrence interval of each section. Abbreviation: MRI: Mean Recurrence Interval; ANHF., the Anninghe Fault; DLSF., the Daliangshan Fault; ZMHF., the Zemuhe Fault; XJF N., the North Section of Xiaojiang Fault; XJF M., the Middle Section of Xiaojiang Fault; XJF S., the South Section of Xiaojiang Fault.

In general, Figure 6 indicates that the occurrence intervals of strong earthquakes vary in time scale with different recurrence pattern. For the same fault, occurrence intervals can range from tens to thousands of years, which are characterized by short-term strong earthquakes recurrence and long quiet period recovery.

1. **Frequency-magnitude relation**

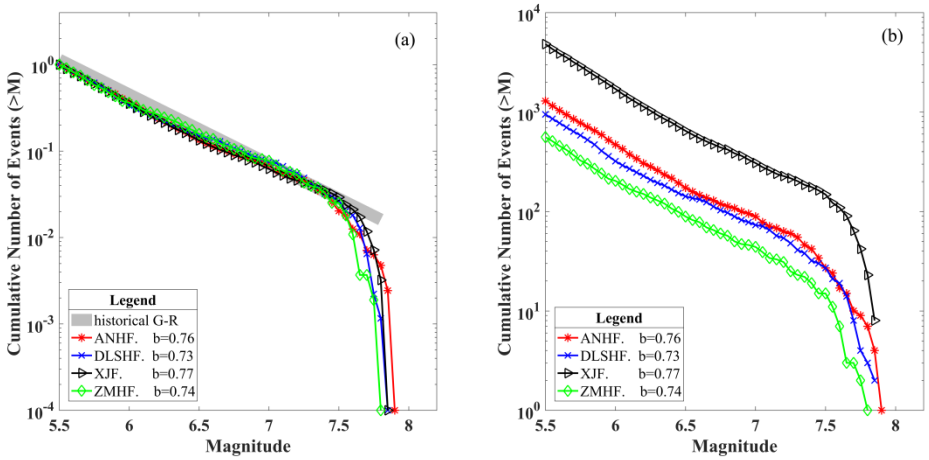

Figure 7 The cumulative number versus magnitude distributions of each fault. (a)**:** normalized number; (b)**:** original number. The magnitude interval is 0.05. Fault abbreviation: ANHF., the Anninghe Fault; DLSF., the Daliangshan Fault; ZMHF., the Zemuhe Fault, XJF., the Xiaojiang Fault.

In section 3.4, the G-R relation of the synthetic seismic catalog has been ascertained by optimizing the model parameter whose b-value consistent with that of the historical earthquakes. For validation of the synthetic seismic catalog, we also acquire the frequency-magnitude relation of each fault (Figure 7). As shown in the Figure 7a, the differences in b-values of four faults are well within the acceptable limits. Meanwhile, the frequency-magnitude relation of single fault is compatible with the historical G-R relation of AZDX fault zone, which further suggests the rationality of the simulated seismic catalog. From the Figure 7a, what we can obtain is that the maximum magnitude earthquake occurs in the Anninghe fault as well. And the maximum magnitude earthquake of Zemuhe fault is the smaller than that of other faults. In the Figure 7b, the number of earthquakes on the Xiaojiang fault is significantly larger than other faults, which may be related to the strong seismicity and the long fault span. The length of the Zemuhe fault is almost similar to that of the Anninghe fault, but the number of earthquakes in the Zemuhe is the least, indicating lower seismicity. The cumulative number-magnitude distribution of the Anninghe fault is closest to the Daliangshan fault, while the length of the Daliangshan fault is twice as long as that of the Anninghe fault.

1. **Discussions**

   (a) **Model parameters uncertainties on simulation results**

In section 3.4, we defined that reasonable value range of dynamic trigger factor and stress drop factor, which are 0.7~0.9 and 0.5~0.7. Tuning the value of dynamic trigger factor M corresponding to fixing stress drop factor value, the Figure 8 illustrates their effects on frequency magnitude distributions of synthetic

catalogs. In order to facilitate comparison, curves in Figure 8 have been normalized. All the frequency-magnitude distributions using different stress drop factors and dynamic trigger factors setting are in agreement with the historical seismic catalog under the M7.

With the stress drop factor value of 0.5 (Figure 8a), varying the value of the dynamic trigger factor η from 0.7 to 0.9 seems to have slight influence on the frequency magnitude distributions of synthetic catalogs. The cumulative number of earthquakes larger than M7.5 drops dramatically. When fixing the stress at 0.6 (in Figure 8b), the distribution curves of the frequency magnitude with dynamic trigger factor value of 0.7 and 0.8 almost coincide and suit the historical seismic catalog well below M7. And the frequency magnitude curve of the stress drop factor value at 0.6 harmonizes better below M7.5. In the Figure 8c, with the stress drop factor value of 0.7, fixing the dynamic trigger factor at 0.8 and 0.9 fits the distributions of M7~M7.5earthquakes in historical seismic catalog well, but diminishes the amount of M6~M6.5. The earthquake number lager than M6.5 displays in a steeper slope. Through the Figure 8, we also notice that the dynamic trigger factor also affects the maximum magnitude in some degree.

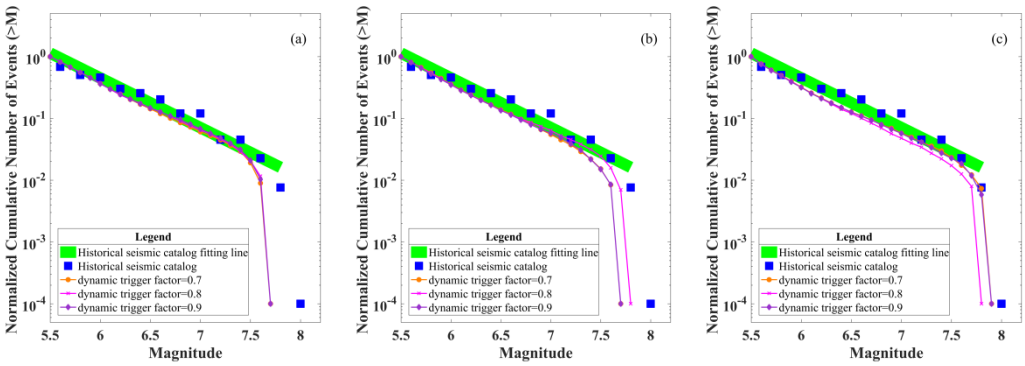

Figure 8 the normalized frequency magnitude distribution with different combinations of stress drop factor and dynamic trigger factor. Subplot (a), (b), (c) correspond to the stress drop factor value of 0.5, 0.6 and 0.7, respectively. The blue diamonds symbolize the normalized cumulative number of observed seismic events, which is represented by the green bold line. The thin lines with markers are the frequency magnitude distributions of synthetic catalogs associated with different values of dynamic trigger factor η. The magnitude interval of synthetic catalog is 0.1.

The frequency magnitude distributions with different tuning parameter (η, M) combinations generally approximate the G-R relation of historical seismic catalog properly in the straight section of frequency magnitude curve, but exhibit deviation from the curve corner to the maximum magnitude. As stated above, the stress drop factor governs the maximum magnitude of the synthetic cata-

log. Increasing the stress drop factor, the maximum magnitude in the frequency magnitude distribution also increases.

For earthquakes before 1900, the magnitudes can't be measured instrumentally. When compiling the historical earthquake catalog, the epicenter intensity is determined according to historical material, and the magnitude is evaluated by the magnitude-intensity empirical equation (Department of Earthquake Disaster Prevention, 1995). However, due to a variety of factors, the historical intensity recorded may be larger than actual one. For example, the disaster situation may be exaggerated in record, which leads to the overestimations of the historical earthquake magnitudes. In the historical seismic catalog of AZDX fault zone, 17 earthquakes are greater than M7, 13 of which are recorded before 1900. The largest magnitude earthquake in the AZDX fault zone is the 1833 Songming M8 (Shen *et al.*, 2003). Considering that magnitude evaluation derived from historical records may be larger than actual, the combination of a stress drop factor of 0.6 and a dynamic trigger factor of 0.8 is acceptable reasonably for the AZDX model.

1. **Seismic Hazard Assessment**

Assessing seismic hazard of future strong earthquakes is a critical problem in seismology. Based on the synthetic catalog simulated by the VQ, we have evaluated seismic hazard of the AZDX fault system. We have collected the latest earthquakes verified by paleoearthquake investigation or historical record, and refer to the occurrence interval probability of successive strong earthquakes. Typically, a relatively short occurrence interval and a long elapsed time favor a higher seismic hazard, and vice versa. We have qualitatively analyzed seismic hazard of each fault as follows. It should be noted that this kind of qualitative analysis may underestimate seismic hazard due to stochastic process of earthquakes.

ANHF

Researchers has prospered that the Anninghe fault is in the strong seismic risk with the accumulated moment magnitude is larger than M7 (Wen *et al.*, 2008a; Yao and Yang). Some studies suggest that the southern section of Anninghe fault identified with remarkable inter-seismic fault slip deficits (Li *et al.*, 2021). But it's believed that the risk of strong earthquakes in the southern section of Anninghe fault is not as high as that in the northern section (Ran *et al.*, 2008b). In the north section of the Anninghe fault, with average strong seismic recurrence interval more than 1000a, the latest strong seismic event has been identified occurring in the 1480 with magnitude M7.5±0.3. Therefore, the seismic hazard of the Anninghe fault is moderate.

ZMHF

The last strong earthquake on the Zemuhe fault occurred in 1850 (He and Oguchi, 2008; Ren and Li, 1993; Wang *et al.*, 2013; Wang *et al.*, 2014). According to the co-seismic displacement, the magnitude of the latest strong seismic

event is estimated larger than M7 via empirical scaling relation (Wen *et al.*, 2000). Considering the long recurrence interval of the Zemuhe fault, the seismic hazard of the Zemuhe fault is relatively low.

DLSF

Four exploration trenches were excavated along secondary faults of the Daliangshan fault zone, and nine paleoseismic events of magnitude 7 or above were revealed by these trenches (Song *et al.*, 2002). In the section of Shimian-Yuexi and Zhaojue, the elapsed time is far less than the simulated mean strong seismic recurrence interval. It is proposed that the penultimate paleoseismic event occurring in 3050±240aBP yields an estimated magnitude of 7.5 by empirical scaling laws between magnitude and slip (WC94). For the Puxiong section corresponding to 60~120 km section, the mean recurrence interval of strong earthquakes is about 3267~5199a which suggests that the elapse time is closed to the lower bound of the mean strong recurrence interval.

Only one simulated earthquake in the Jiaojihe section is obtained and the mean strong seismic recurrence interval cannot be obtained, which indicates that the mean strong seismic recurrence interval of the Jiaojihe can reach up to ten thousand years scale.

However, the seismic hazards of faults with low seismic activities are typically underestimated, such as for the Longmenshan fault which generated the unexpected M8.0 Wenchuan earthquake. Based on slip rates and the elapsed times since the most recent events along the Jiaojihe and Butuo sections of the DLSF, seismic energy equivalent to M ~ 7.6 may be accumulated, suggesting a significant seismic hazard to the DLSF (Sun *et al.*, 2019b).

XJF

The Xiaojiang fault has experienced a lot of strong earthquakes in history. The latest event is the 1733 M7.75 Dongchuan earthquake on the middle northern part of the Xiaojiang fault, and the 1789 Huaning M7 on the southern part. The largest one on the Xiaojiang fault is the 1833 Songming M8.0 earthquake, which located on the middle part of the Xiaojiang fault. Due to the relatively short recurrence interval of the Xiaojiang fault, the seismic hazard of the Xiaojiang fault should be high. However, considering the elapsed times of latest events are short, the seismic hazard of the Xiaojiang fault should be relatively low. Thus, a more comprehensive investigation of the seismic hazard of the Xiaojiang fault is needed to draw a reliable conclusion, but is beyond the scope of this study.

1. **Scaling relation plots**

For regional and global seismic hazard analyses, various visions of empirical relationships related magnitude to fault rupture parameters have been developed (Konstantinou, 2014; Leonard, 2010; Wells and K. J. Coppersmith, 1994). It has been known that the WC94 are commonly applied in previous studies. However, the purely empirical WC94 relations are not self-consistent especially for reverse (thrust) faults (Leonard, 2010). And for the intraplate regions, the WC94

dataset doesn't include plenty of earthquakes (Cheng *et al.*, 2019; Leonard, 2010). Leonard (2010) proposes new self-consistent scaling relations which all the rupture parameters are consistent with the definition of seismic moment (hereafter Leonard2010). The dataset of the Leonard2010 and WC94 are collected worldwide. In the view of the special tectonic environment, some scaling relations within mainland China have been presented (Cheng *et al.*, 2019; Deng *et al.*, 1992; Wang *et al.*, 2011a). Among them, Cheng *et al.* (2019) develops the more detailed magnitude rupture parameters scaling relations distinguishing the western and eastern China.

For model validation, we also derive the moment-rupture and the rupture area-slip regression relations from the synthetic seismic catalog (M 4.8). In the Figure 9, the scale relation from the simulated seismic catalog appears as two parallel gray dotted branched lines. For western China, Cheng *et al.* (2019) presented detailed scaling relation with segmented linearity. From the M4.8 to M6.7, the above gray dotted line shows excellent consistency with the regression relation of strike-slip fault. The slope of the scaling relation with M 6.7 is less than that in the interval of 4.8 magnitude <6.7. It means that the scaling relation of the simulated seismic catalog does not match with that developed by Cheng *et al.* (2019) for earthquakes with M 6.7. The below gray dotted line coincides great with the WC94 scaling relation. For the same moment magnitude, the corresponding rupture area concluded from the simulated seismic catalog is obviously larger than that regressed by the Leonard (2010).

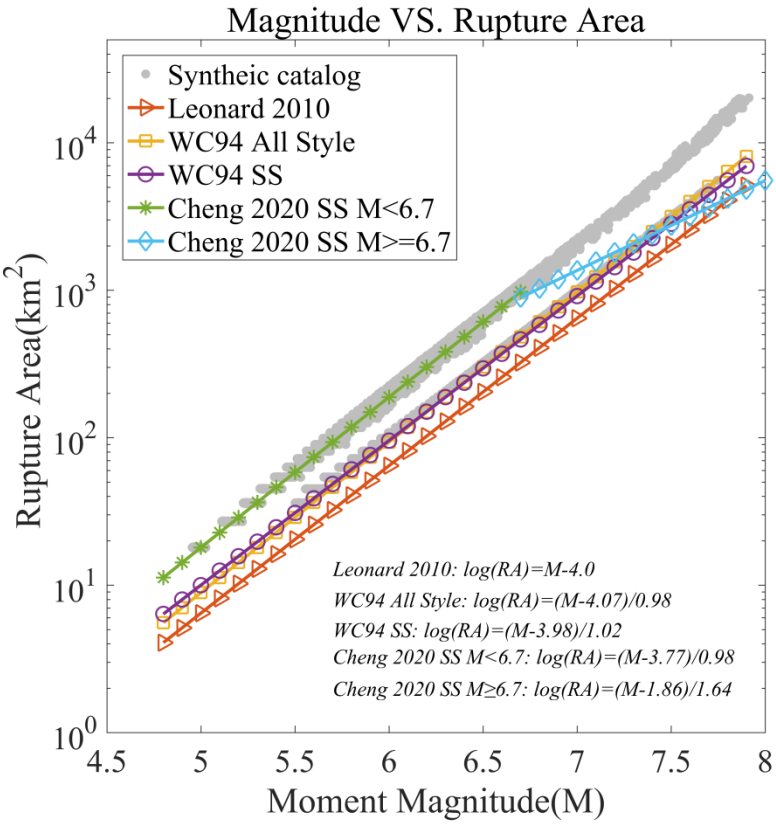

Figure 9 Scale relations of Rupture Area (RA) relative to Moment Magnitude (M) from different researchers. The gray dot is scale relation of rupture area versus moment magnitude from synthetic catalog. The formulas in the lower right corner indicate the empirically mathematical expressions with different sources. Leonard2010 is the regressed scaling relation by Leonard (2010). WC94 all styles indicates the scaling relation from all types of earthquake dataset including Strike-Slip (SS), reverse-slip and normal-slip (Wells and K. J. Coppersmith, 1994). Cheng2020 represents the empirical scaling relation regressed by Cheng *et al.* (Cheng *et al.*).

There are two branches in the statistical curve of scaling relations from the simulated seismic catalog (Figure 9). The reason of this phenomenon is due to the boundary effect of the fault model. The slip rates of elements nearby the fault geometry boundary are adjusted equally to that of the center element when constructing the fault model. When earthquake occurs closed to geometric boundary of the model, the rupture cannot propagate freely. In the further work, special treatment should be carried out on the fault geometry boundary, such as weakening the slip rate on the element neighboring the boundary.

1. **Limitations**

To valid our simulation, we compare the synthetic catalog with paleoearthquakes. However, this comparison is limited by several issues related to records of paleoearthquakes. Due to missing and small number of paleoearthquakes, uncertainties of occurrences of the paleoearthquakes are typically as large as tens to hundreds of years, which are comparative to recurrence intervals of synthetic earthquakes. Such large uncertainties weaken the validation of simulation using paleoearthquakes.

In our simulation, the rupture model is straightforward and simple. However, several studies have shown that the Anninghe fault exhibits complex rupture behavior, such as cascade rupture(Wang *et al.*, 2014). Besides, heterogeneities in fault geometry, crust properties, and stress distributions along the fault system are also critical factor controlling the rupture process (Yao and Yang, 2021). However, for a long period simulation in a multiple-fault system, considering all factors above mentioned is difficult. This study aims to provide statistical features of strong earthquakes in a complex region and we ignore those factors for simplicity.

1. **Conclusion**

Based upon the fault slip rates and geometry in the AZDX fault system, southwestern China, we construct a 3D fault model for the AZDX fault zone. By applying the physic-based model (VQ) which considers the interaction between faults, we get a 20,000a synthetic earthquake catalog. Then the recurrence intervals of strong earthquakes (M 7) in the simulated catalog are extracted, which are mostly in good agreement with those of paleoearthquakes and historical earthquakes. Subsequently, the occurrence interval probability of successive strong earthquakes in each fault is also presented to help evaluate seismic hazards. Our results show that the simulated catalog is consistence with the observed seismicity in spatial distribution of large earthquakes, b value and mean seismic rate. The mean intervals of M 7.0 earthquakes for the Anninghe, Zemuhe, Daliangshan and Xiaojiang faults are 299a, 867a, 361a, and 90a, respectively. Our results provide a useful tool to evaluate seismic hazard in a complicated region.

Acknowledgement

We appreciate Yongsheng Zhou for help constructing the fault model. This research is jointly supported by National Natural Science Foundation of China projects (U2139205, 41804048, U2039204), the National Key R&D Program of China (2018YFC1503400), the China Postdoctoral Science Foundation (2020M673469), and the Special Fund of the Institute of Geophysics, China Earthquake Administration (DQJB 22Z01-09). Some figures are plotted with Generic Mapping Tool mapping software (Wessel and Smith, 1991).

Data Availability Statement

The observed and historical catalogs are from China Earthquake Network Center

and Department of Earthquake Disaster Prevention, China Earthquake Administration (Department of Earthquake Disaster Prevention). The slip rates of the AZDX faults are obtained from Li *et al.* (2021).

References

Ben-Zion, Y. (1996), Stress, slip, and earthquakes in models of complex single-fault systems incorporating brittle and creep deformations, *Journal of Geophysical Research: Solid Earth*, *101*(B3), 5677-5706.Chen, R., and P. Li (1988), Slip rates and earthquake recurrence intervals of the western branch of the Xiaojiang fault zone (in Chinese), *Seismology and Geology*, *10*(2), 3-15.Cheng, J., J. Liu, W. Gan, H. Yu, and G. Li (2011), Characteristics of strong earthquake evolution around the eastern boundary faults of the Sichuan-Yunnan rhombic block (in Chinese), *Science China Earth Sciences*, *54*(11), 14.Cheng, J., Y. Rong, H. Magistrale, G. Chen, and X. Xu (2019), Earthquake rupture scaling relations for mainland China, *Seismological Research Letters*, *91*(1), 248-261, doi:10.1785/0220190129.Christophersen, A., D. A. Rhoades, and H. V. Colella (2017), Precursory seismicity in regions of low strain rate: insights from a physics-based earthquake simulator, *Geophysical Journal International*, *209*(3), 1513-1525.Console, R., R. Carluccio, M. Murru, E. Papadimitriou, and V. Karakostas (2021), Physics-Based Simulation of Spatiotemporal Patterns of Earthquakes in the Corinth Gulf, Greece, Fault System, *Bulletin of the Seismological Society of America*.Console, R., M. Chiappini, L. Minelli, F. Speranza, R. Carluccio, and M. Greco (2018), Seismic hazard in southern Calabria (Italy) based on the analysis of a synthetic earthquake catalog, *Acta Geophysica*, *66*(5), 931-943.Crone, A. J., and K. M. Haller (1991), Segmentation and the coseismic behavior of basin and Range normal faults: examples from east-central Idaho and southwestern Montana, U.S.A, *Journal of Structural Geology*, *13*(2), 151-164.Deng, Q., G. Yu, and W. Ye (1992), Study on the relations between parameters of surface rupture and magnitude, in, *Research on Active Fault (in Chinese)*, *2*.Deng, Q., P. Zhang, Y. Ran, X. Yang, W. Min, and Q. Chu (2003a), Basic characteristics of active tectonics of China, *Sci. China Ser. D-Earth Sci.*, *46*(4), 356-372.Deng, Q., P. Zhang, Y. Ran, X. Yanmg, W. Ming, and Q. Chu (2003b), Basic characteristics of active tectonics of China (in Chinese), *Science China Earth Sciences*.Department of Earthquake Disaster Prevention, C. E. A. (1995), *Catalogue of Chinese historical strong earthquakes (the 23rd century B.C. to 1911, in Chinese)*, Seismological Press.Department of Earthquake Disaster Prevention, C. E. A. (1999), *Catalogue of Chinese modern earthquakes (1912 to 1990, Ms 4.7, in Chinese)*, Seismological Press.Field, E. H. (2019), How physics-based earthquake simulators might help improve earthquake forecasts, edited, Seismological Society of America.Gao, W., H. He, H. Sun, and Z. Wei (2016), Paleoearthquakes along Puxiong Fault of Daliangshan fault zone during Late Quaternary (in Chinese), *Seismology and Geology*.Hanks, T. C., and W. H. Bakun (2002), A Bilinear Source-Scaling Model for M-log A Observations of Continental Earthquakes, *Bulletin of the Seismological Society of America*, *92*, 1841-1846.He, H., and T. Oguchi (2008), Late Quaternary activity of the Zemuhe and Xiaojiang faults in southwest China from geomor-

phological mapping, *Geomorphology*, *96*(1-2), 62–85.Hou, Y., X. Jin, and S. Zhou (2020), Update and test of a seismicity simulation program based on the Coulomb-Navier failure criterion and the stress transfer mechanism, *Pure and Applied Geophysics*, *177*(1), 233-246.Jiang, G., X. Xu, G. Chen, Y. Liu, and Y. Fukahata (2015a), Geodetic imaging of potential seismogenic asperities on the Xianshuihe-Anninghe-Zemuhe fault system, southwest China, with a new 3-D viscoelastic interseismic coupling model, *Journal of Geophysical Research: Solid Earth*, *120*(3).Jiang, G., X. Xu, G. Chen, Y. Liu, Y. Fukahata, H. Wang, G. Yu, X. Tan, and C. Xu (2015b), Geodetic imaging of potential seismogenic asperities on the Xianshuihe-Anninghe-Zemuhe fault system, southwest China, with a new 3-D viscoelastic interseismic coupling model, *Journal of Geophysical Research: Solid Earth*, *120*(3), 1855-1873.Kanamori, H., and D. L. Anderson (1975), Theoretical basis of some empirical relations in seismology, *Bulletin of the Seismological Society of America*, *65*(5), 1073-1095.Khodaverdian, A., H. Zafarani, and M. Rahimian (2016a), Long term fault slip rates, distributed deformation rates and forecast of seismicity in the Iranian Plateau, *Tectonics*, *34*(9-10), 2190-2220.Khodaverdian, A., H. Zafarani, K. Schultz, and M. Rahimian (2016b), Recurrence time distributions of large earthquakes in Eastern Iran, *Bulletin of the Seismological Society of America*, *106*(6), 2624-2639.Konstantinou, K. I. (2014), Moment magnitude-Rupture area scaling and stress-drop variations for earthquakes in the Mediterranean region, *Bulletin of the Seismological Society of America*, *104*, 2378–2386.Leonard, M. (2010), Earthquake fault scaling: self-consistent relating of rupture length, width, average displacement, and moment release, *Bulletin of the Seismological Society of America*, *100*(5A), 1971-1988.Li, H., M. Hao, S. Song, L. Zhu, D. Cui, W. Zhuang, F. Yang, and Q. Wang (2021), Interseismic fault slip deficit and coupling distributions on the Anninghe-Zemuhe-Daliangshan-Xiaojiang fault zone, southeastern Tibetan Plateau, based on GPS measurements, *Journal of Asian Earth Sciences*, *219*.Li, X., Y. Ran, F. Wu, X. Ma, and J. Cao (2018), Rupture characteristics of Late Quaternary strong earthquakes on the western branch of the Xiaojiang fault zone (in Chinese), *Seismology and Geology*, *40*(6), 1179-1203.Li, Y., M. Hao, L. Ji, and S. Qin (2014), Fault slip rate and seismic moment deficit on major active faults in mid and south part of the Eastern margin of Tibet plateau (in Chinese), *Chinese Journal of Geophysics*, *54*(4), 1062-1078.Liu, M., and S. Stein (2011), Aftershocks, in *Encycopedia of Solid Earth Geophysics*, edited by H. K. Gupta, pp. 192-194, Springer Dordrecht.Mao, Z. (2001), The activity of the south segment of Xiaojiang fault in late Quaternary (in Chinese), China University of Geosciences (Beijing).Ogata, Y. (1988), Statistical Models for Earthquake Occurrences and Residual Analysis for Point Processes, *Journal of the American Statistical Association*, *83*(401), 9-27.Okada, Y. (1992), Surface Deformation due to Shear and Tensile Faults in a Half Space, *Bulletin of the Seismological Society of America*, *82*(2), 1018-1040.Pollitz, F. F. (2012), ViscoSim earthquake simulator, *Seismological Research Letters*, *83*(6), 979-982.Qian, H. (1992), Research on the recent surficial faulting on the northern segment of the Anninghe Fault Zone and earthquake potential (in Chinese), *Seismology and Geology*.Ran, Y., L. Chen, J. Cheng, and H. Gong (2008a), Late Quaternary

surface deformation and rupture behavior of strong sarthquake on the eegment north of Mianning of the Anninghe fault (in Chinese), *Science China Earth Sciences*(9), 14.Ran, Y. K., J. Cheng, H. Gong, and L. Chen (2008b), Late quaternary geomorphic deformation and displacement rates of the Anninghe Fault around Zimakua, *Seismology and Geology*.Ren, J., and P. Li (1993), The characteristics of surface faulting of the 1850 earthquake in Xichang, Sichuan (in Chinese), *Seismology and Geology*.Richards-Dinger, K., and J. H. Dieterich (2012), RSQSim earthquake simulator, *Seismological Research Letters*, *83*(6), 983-990.Robinson, R., and R. Benites (1996), Synthetic seismicity models for the Wellington region, New Zealand: Implications for the temporal distribution of large events, *Journal of Geophysical Research: Solid Earth*, *101*(B12), 27833-27844.Rundle, J. B., J. R. Holliday, W. R. Graves, D. L. Turcotte, K. F. Tiampo, and W. Klein (2012), Probabilities for large events in driven threshold systems, *Physical Review*, *86*(2), 1-6.Rundle, J. B., and W. Klein (1995), Dynamical segmentation and rupture patterns in a "toy" slider-block model for earthquakes, *Nonlinear Processes in Geophysics*, *2*(2), 61-79.Rundle, J. B., P. B. Rundle, A. Donnellan, and G. Fox (2004), Gutenberg-Richter statistics in topologically realistic system-level earthquake stress-evolution simulations, *Earth, Planets and Space*, *56*(8), 761-771.Rundle, P. B., J. B. Rundle, K. F. Tiampo, A. Donnellan, and D. L. Turcotte (2006), Virtual California: Fault Model, Frictional Parameters, Applications, *Pure and Applied Geophysics*, *163*(9), 1819-1846.Rundle, P. B., J. B. Rundle, K. F. Tiampo, J. Martins, S. Mcginnis, and W. Klein (2001), Nonlinear Network Dynamics on Earthquake Fault Systems, *Physical Review Letters*.Sachs, M. K., E. M. Heien, D. L. Turcotte, M. B. Yikilmaz, J. B. Rundle, and L. H. Kellogg (2012), Virtual California earthquake simulator, *Seismological Research Letters*, *83*(6), 973-978.Schultz, K. W., M. R. Yoder, J. M. Wilson, E. M. Heien, M. K. Sachs, J. B. Rundle, and D. L. Turcotte (2018), Parametrizing physics-based earthquake simulations, in *Earthquakes and Multihazards Around the Pacific Rim, Vol. I*, edited, pp. 75-84, Springer.Schwartz, D. P., and K. J. Coppersmith (1984), Fault behavior and characteristic earthquakes: examples from the Wasatch and San Andreas Fault Zones, *Journal of Geophysical Research Solid Earth*, *89*(B7), 5681-5698.Shaw, B. E., K. R. Milner, E. H. Field, K. Richards-Dinger, J. J. Gilchrist, J. H. Dieterich, and T. H. Jordan (2018), A physics-based earthquake simulator replicates seismic hazard statistics across California, *Science advances*, *4*(8), eaau0688.Shen, J., and Y. Wang (1999), Estimation of seismic risk of the Xiaojiang active fault zone using slip rate (in Chinese).Shen, J., Y. Wang, and F. Song (2003), Characteristics of the active Xiaojiang fault zone in Yunnan, China: a slip boundary for the southeastward escaping Sichuan–Yunnan block of the Tibetan plateau, *Journal of Asian Earth Sciences*.Shen, Z., J. Lü, M. Wang, and R. Bürgmann (2005), Contemporary crustal deformation around the southeast borderland of the Tibetan Plateau, *Journal of Geophysical Research*.Somerville, P., K. Irikura, R. Graves, S. Sawada, D. Wald, N. Abrahamson, Y. Iwasaki, T. Kagawa, N. Smith, and A. Kowada (1999), Characterizing Crustal Earthquake Slip Models for the Prediction of Strong Ground Motion, *Seismological Research Letters*.Song, F., R. Li, and X. Xu (2002), Preliminary results of the investigation of paleo-earthquakes

along the daliangshan fault zone, sichuan province, China (in Chinese), *Seismology and Geology*, *24*(1), 27-34.Song, F., and Y. Wang (1998), *The Xiaojiang Active Fault Zone (in Chinese)*, Seismological Press, Beijing.Stein, R. S. (2000), The role of stress transfer in earthquake occurrence, *Translated World Seismology*, *402*(6762), 605-609.Sun, H., H. He, and Y. Ikeda (2019a), Paleoearthquake History Along the Southern Segment of the Daliangshan Fault Zone in the Southeastern Tibetan Plateau, *Tectonics*, *38*(7).Sun, H., H. He, Y. Ikeda, Z. Wei, C. Chen, Y. Xu, F. Shi, L. Bi, Y. Shirahama, and S. Okada (2019b), Paleoearthquake history along the southern segment of the Daliangshan fault zone in the southeastern Tibetan Plateau, *Tectonics*, *38*(7), 2208-2231.Sun, H. Y., H. He, Z. Wei, and W. Gao (2015), Late quaternary activity of zhuma faulton the north segment of daliangshan fault zone (in Chinese), *Seismology and Geology*, *37*(2), 440-454.Sun, Y., G. Luo, C. Hu, and Y. Shi (2020), Preliminary analysis of earthquake probability based on the synthetic seismic catalog, *Science China Earth Sciences*, *63*(7), 985-998.Tapponnier, P., G. Peltzer, A. Dain, R. Armijo, and P. Cobbold (1982), Propagating extrusion tectonics in Asia: New insights from simple experiments with plasticine, *Geology*, *10*(12), 611.Tullis, T. E. (2012), Preface to the focused issue on earthquake simulators, *Seismological Research Letters*, *83*(6), 957-958.Tullis, T. E., K. Richards-Dinger, M. Barall, J. H. Dieterich, E. H. Field, E. M. Heien, L. H. Kellogg, F. F. Pollitz, J. B. Rundle, and M. K. Sachs (2012), A comparison among observations and earthquake simulator results for the allcal2 California fault model, *Seismological Research Letters*, *83*(6), 994-1006.Wan, Y. (2016), *Introduction to Seismology (in Chinese)*, Science Press.Wang, H. (2013), Study on recurrence and correlation of great earthquakes on anninghe-Zemuhe fault zone in western Sichuan (in Chinese), *Recent Developments in World Seismology*.Wang, H., M. Liu, J. Cao, X. Shen, G. Zhang, J. M. Wilson, M. R. Yoder, J. B. Rundle, D. L. Turcotte, and K. W. Schultz (2011a), Slip rates and seismic moment deficits on major active faults in mainland China, *Journal of Geophysical Research: Solid Earth*, *116*(B2), doi:10.1029/2010JB007821.Wang, H., Y. Ran, Y. Li, and L. Chen (2013), Paleoseismic ruptures and evolution of a small triangular pull-apart basin on the Zemuhe fault (in Chinese), *Science China Earth Sciences*(3), 9.Wang, H., Y. Ran, Y. Li, F. Gomez, and L. Chen (2014), A 3400-year-long paleoseismologic record of earthquakes on the southern segment of Anninghe fault on the southeastern margin of the Tibetan Plateau, *Tectonophysics*, *628*, 206-217.Ward, S. N. (2012), ALLCAL earthquake simulator, *Seismological Research Letters*, *83*(6), 964-972.Wei, Z., H. He, F. Shi, Y. Xu, L. Bi, and H. Sun (2012), Slip rate on the south segment of Daliangshan fault zone (in Chinese), *Seismology and Geology*(2), 282-293.Wells, D. L., and K. J. Coppersmith (1994), New empirical relationships among magnitude, rupture length, rupture width, rupture area, and surface displacement, *Bullctin of the Seismological Society of America*, *84*(4), 974-1002.Wen, X., S. Ma, X. Xu, and Y. He (2008a), Historical pattern and behavior of earthquake ruptures along the eastern boundary of the Sichuan-Yunnan faulted-block, southwestern China, *Physics of the Earth and Planetary Interiors*, *168*(1-2), 16-36.Wen, X. (1993), Fracture segmentation and seismic potential probability estimation of Xiaojiang fault zone, *Acta Seismolog-*

ica Sinica.Wen, X., P. Du, and D. Li (2000), New evidence of paleoearthquakes and date of the latest event on the xiaoxiangling mountain segment of the anninghe fault zone (in Chinese), *Seismology and Geology*.Wen, X., J. Fan, G. Yi, Y. Deng, and F. Long (2008b), A seismic gap on the Anninghe fault in western Sichuan, China, *Science China Earth Sciences*(10), 13.Wessel, P., and W. H. F. Smith (1991), Free software helps map and display data, *Eos Trans. AGU*, *72*(41), 441-446, doi:10.1029/90eo00319.Xu, X., Q. Deng, X. Xu, C. Xu, G. Yu, X. Wu, and J. Zhang (1996), Nonlinear characteristics of paleoseismicity in China, *Journal of Geophysical Research: Solid Earth*, *101*(B3), 6209-6231,doi: 10.1029/95JB01238.Xu, X., X.Wen, R. Zheng, W. Ma, F. Song, and G. Yu (2003), Pattern of latest tectonic motion and its dynamics foractive blocks in S ichuan-Yunnan region, China (in Chinese), *Science China Earth Sciences*, *33*(B04), 12.Yao, S., and H. Yang (2021), Hypocentral dependent shallow slip distribution and rupture extents along a strike-slip fault, *Earth and Planetary Science Letters*, 117296, doi:https://doi.org/10.1016/j.epsl.2021.117296.Yoder, M. R., K. W. Schultz, E. M. Heien, J. B. Rundle, D. L. Turcotte, J. W. Parker, and A. Donnellan (2015), The Virtual Quake earthquake simulator: a simulation-based forecast of the El Mayor-Cucapah region and evidence of predictability in simulated earthquake sequences, *Geophysical Supplements to the Monthly Notices of the Royal Astronomical Society*, *203*(3), 1587-1604.Zhao, J., Z. Jiang, A. Niu, and Y. Wu (2015), Study on dynamic characteristics of fault locking in the eastern boundary of the Sichuan-Yunnan Rhombic Block, *Chinese Journal of Geophysics*, *58*(3), 872-885.Zhou, S. (2008), Seismicity simulation in Western Sichuan of China based on the fault interactions and its implication on the estimation of the regional earthquake risk, *Chinese Journal of Geophysics*, *51*(1), 132-142.Zhou, S., S. Johnston, R. Robinson, and D. Vere-Jones (2006), Tests of the precursory accelerating moment release model using a synthetic seismicity model for Wellington, New Zealand, *Journal of Geophysical Research: Solid Earth*, *111*(B5).Zöller, G., and Y. Ben-Zion (2014), Large earthquake hazard of the San Jacinto fault zone, CA, from long record of simulated seismicity assimilating the available instrumental and paleoseismic data, *Pure and Applied Geophysics*, *171*(11), 2955-2965.